

## Effects of Graphene/Silver Nanocomposite on the Microstructure of Amorphous Mg-based Hydride

Huang Lin-jun<sup>\*</sup>, Wang Yan-xin<sup>\*</sup>, Tang Jian-guo<sup>\*</sup>, Wang Yao, Liu Ji-xian, Jiao Ji-qing, Wang Wei

College of Materials Science and Engineering, Qingdao University, Qingdao 266071, China

\*E-mail: [newboy66@126.com](mailto:newboy66@126.com), [yanxin\\_2008@126.com](mailto:yanxin_2008@126.com), [tang@qdu.edu.cn](mailto:tang@qdu.edu.cn)

Received: 7 July 2016 / Accepted: 22 September 2016 / Published: 10 November 2016

---

The influence of a graphene/silver (G/A) nanocomposite coating layer on the microstructural evolution and surface oxidation of a Mg–Ni–La hydride is investigated systematically by XRD, SEM, EDS and HRTEM in detail. SEM and EDS reveal that the existence of the G/A composite prevents the electrode from pulverizing and oxidizing. The oxygen content in the surface of the electrode is reduced from 21.26% to 9.83% after 50 cycles for a Mg–Ni–La electrode with 0.2 mass fraction of G/A. HRTEM shows that the amorphous electrodes with no G/A coating are almost all crystallized, and that the stable Mg<sub>2</sub>NiH<sub>4</sub>, α-Mg, MgH<sub>2</sub> and LaH<sub>2</sub> phases are present with grain sizes as large as 100–120 nm after 50 cycles of charging/discharging. The G/A coating reduces the corrosion and oxidation of the electrode alloy and provides both a pathway for hydrogen diffusion and active sites for the redox reaction of hydrogen. All these factors generate a significant enhancement of the discharge capacity by about 250 mAhg<sup>-1</sup> in each cycle (after activation) for Mg–Ni–La electrodes with 0.2 G/A nanocomposites.

---

**Keywords:** electrode alloy; graphene coating; electrochemical property; surface modification.

### 1. INTRODUCTION

Magnesium-based electrode alloys have attracted increasing attention as electrochemical energy storage and conversion systems in the past 30 years because of their low density, high discharge capacity, and abundant source materials [1-3]. The global magnesium alloy industry has grown to making more than 700,000 tones per year, benefiting the progress of research and production of this technology [4, 5]. However, the industrial application of Mg-based electrodes is inhibited by

their indigent charge/discharge cycle stability induced by the generation of  $\text{Mg}(\text{OH})_2$  on the electrode surface in alkaline solution [6].

Changes in the nanocrystalline and amorphous structures of electrode materials are subjected to close scrutiny to better understand mechanisms of corrosion and oxidation [7-11]. Modification of the surface of hydride particles is a strategy that can be used to protect the base materials and accelerate the electrochemical reaction. In the past several years, surface modification of electrode alloys has been demonstrated to be an efficient way to improve the comprehensive electrochemical performance for the  $\text{Mg}_2\text{Ni}$  electrode alloys. Besides the traditional surface treatment methods, namely alkali, acid and F-treatments that normally affect the surface components of the parent alloy, several groups have reported the improvement in capacity decay of the electrode alloys by microencapsulating the particles with various hybrid coating layers, such as Cu, Co, Ni, polymer, etc. via electroless processes [12-15]. Hybrid coating layers introduced by mechanical milling (MM) have been verified to be efficient in improving the properties of hydride electrodes by preventing corrosion of the disintegrated alloy, leading to superior electrocatalytic activity. Among the commonly used dopants, which include the transition metals, oxides and various carbon sources (graphite, CNTs, carbon black, etc) [16-21], graphene/silver (G/A) composite coating layers exhibit remarkable positive effects on hydrogen absorption and desorption of the  $\text{Mg}_2\text{Ni}$ -type alloy electrodes [22]. This property enhancement has been attributed to the outstanding catalytic activity and electrical conductivity of G/A [22].

In our previous research work, we have prepared a new G/A nanocomposite to improve the anti-corrosion properties of magnesium-based amorphous alloys [22]. This work implies that the G/A nanocomposite can reduce the contact resistance of the electrodes, enhance the electrocatalytic activity of the alloy, and greatly increase the discharge capacity of electrodes. However, the mechanism of surface modification for magnesium-based amorphous alloys using G/A nanocomposite has not been investigated in detail. In this work, the influence of a G/A coating layer on the microstructural evolution and anti-corrosion properties of the Mg–Ni–La hydride is investigated in detail. These results lead to an optimized  $\text{Mg}_2\text{NiH}_4/\text{G/A}$  composite system and provide some insight into the “electrochemical catalytically” enhanced mechanism of the G/A coating layer.

## 2. EXPERIMENTAL

Amorphous Mg-Ni-La electrode ribbons with and without the G/A nanocomposite coating layers were prepared according to the methods reported by our previous study [22]. The crystal structures of the Mg-Ni-La amorphous electrode ribbons that were charged/discharged for different cycle numbers were characterized by a powder X-ray diffractometer (XRD, Philips 1730), with Cu  $K\alpha$  radiation. The microstructure and morphology of the ribbons after charge/discharge cycles were examined by a scanning electron microscope (SEM, JEOL 6460) equipped with an energy-dispersive

X-ray spectrometer (EDS), and by high-resolution transmission electron microscopy (HRTEM, JEOL 2011).

### 3. RESULTS AND DISCUSSION

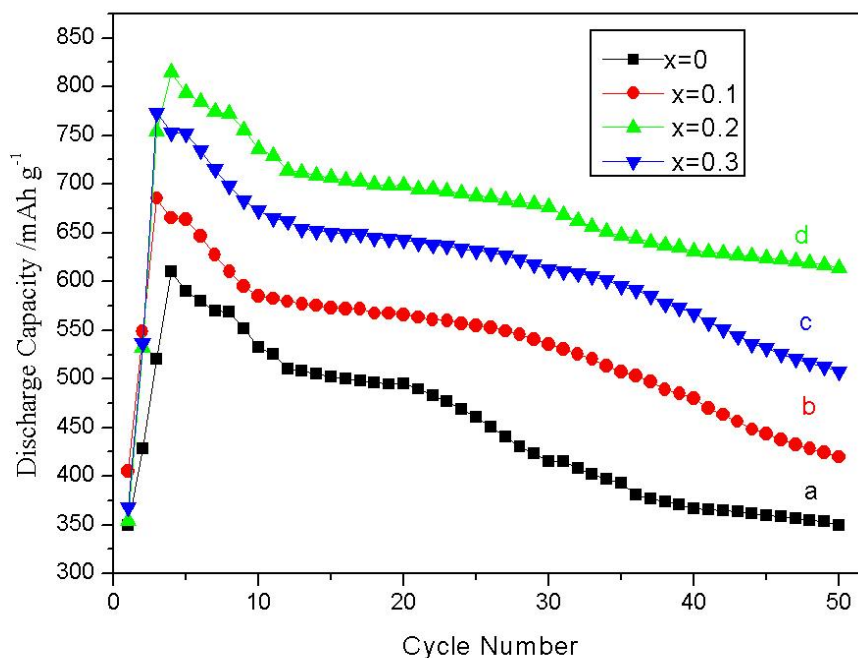


**Figure 1.** Discharge capacities as a function of cycle number for the  $(\text{Mg}_{65}\text{Ni}_{27}\text{La}_8)_x\text{G/A}$  ( $x = 0-0.3$ ) negative electrodes.

Fig. 1 shows the cycle stability of the  $(\text{Mg}_{65}\text{Ni}_{27}\text{La}_8)_x\text{G/A}$  ( $x = 0-0.3$ ) amorphous electrodes obtained in our previous work, where  $x$  is the mass fraction of G/A [22]. The discharge capacities of amorphous electrodes modified with G/A are much higher than that of pure amorphous samples. For all electrodes, the discharge capacity achieved a maximum after 3 or 4 cycles (named activation period), and then decreases for the subsequent cycles. The discharge platform curve becomes smooth after ten cycles.

The increase of the discharge capacity and excellent electrocatalytic activity are believed to result from an increase in the number of active sites for hydrogenation and dehydrogenation on the surface of  $\text{Mg}_{65}\text{Ni}_{27}\text{La}_8$  amorphous alloy. This could be caused by chemical modification of Mg, Ni, and La on the electrode surface [23]. Aymard et al. [24] also reported that fracture of the graphite

layers occurs during ball milling, which would produce some small particles with free dangling bonds. So, we considered that some reactions between the G/A nanoparticles and Mg, Ni, and La atoms on the amorphous electrode may occur, leading to chemical modification on the electrode surface.

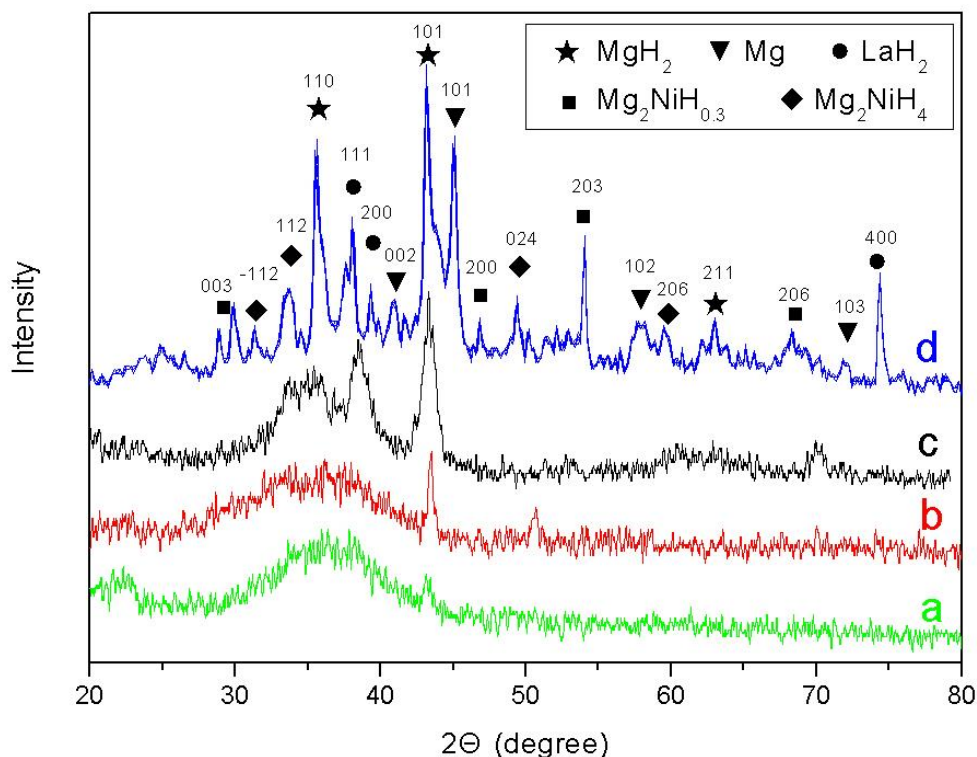


**Figure 2.** XRD patterns of  $\text{Mg}_{65}\text{Ni}_{27}\text{La}_8$  amorphous samples without G/A charged–discharged for: (a) 4 cycles, (b) 10 cycles, (c) 30 cycles and (d) 50 cycles, respectively.

XRD patterns of the  $\text{Mg}_{65}\text{Ni}_{27}\text{La}_8$  amorphous samples after 4, 10, 30 and 50 charge/discharge cycles are shown in Fig. 2. The microstructure remains amorphous phase after 4 cycles, and then gradually crystallizes during the subsequent cycles. Nanocrystalline  $\text{MgH}_2$  and  $\text{Mg}_2\text{NiH}_4$  particles are first detected after the 10<sup>th</sup> cycle (Fig. 2(b)), and nano-size  $\text{Mg}_2\text{NiH}_{0.3}$  and  $\text{LaH}_2$  appears after the 30<sup>th</sup> cycle (Fig. 3(c)). After 50 cycles some stable phases including  $\text{Mg}_2\text{NiH}_4$ ,  $\alpha$ -Mg,  $\text{MgH}_2$ ,  $\text{Mg}_2\text{NiH}_{0.3}$ , and  $\text{LaH}_2$  are present (Fig. 3(d)).

Fig. 3 shows SEM images of  $\text{Mg}_{65}\text{Ni}_{27}\text{La}_8$  amorphous samples without G/A after 0 (a), and 50 charge/discharge cycles (b and c), and the EDS of amorphous electrodes without G/A after 50 charge/discharge cycles (d). From Fig. 3 we can see that particle pulverization occurs on the electrode surface, and most of the surface area is covered with rhabditiform oxide. Also the oxygen content in the electrode surface is 21.26% (Fig. 3(d)) after 50 cycles, indicating that extensive

oxidation/corrosion and particle pulverization of the active electrode occur during charge-discharge cycling. Liao et al. [25] attributed the fast discharge-capacity degradation of Mg-based alloys to the oxidation/corrosion of Mg and La, and the large  $V_H$  in the hydride phase.

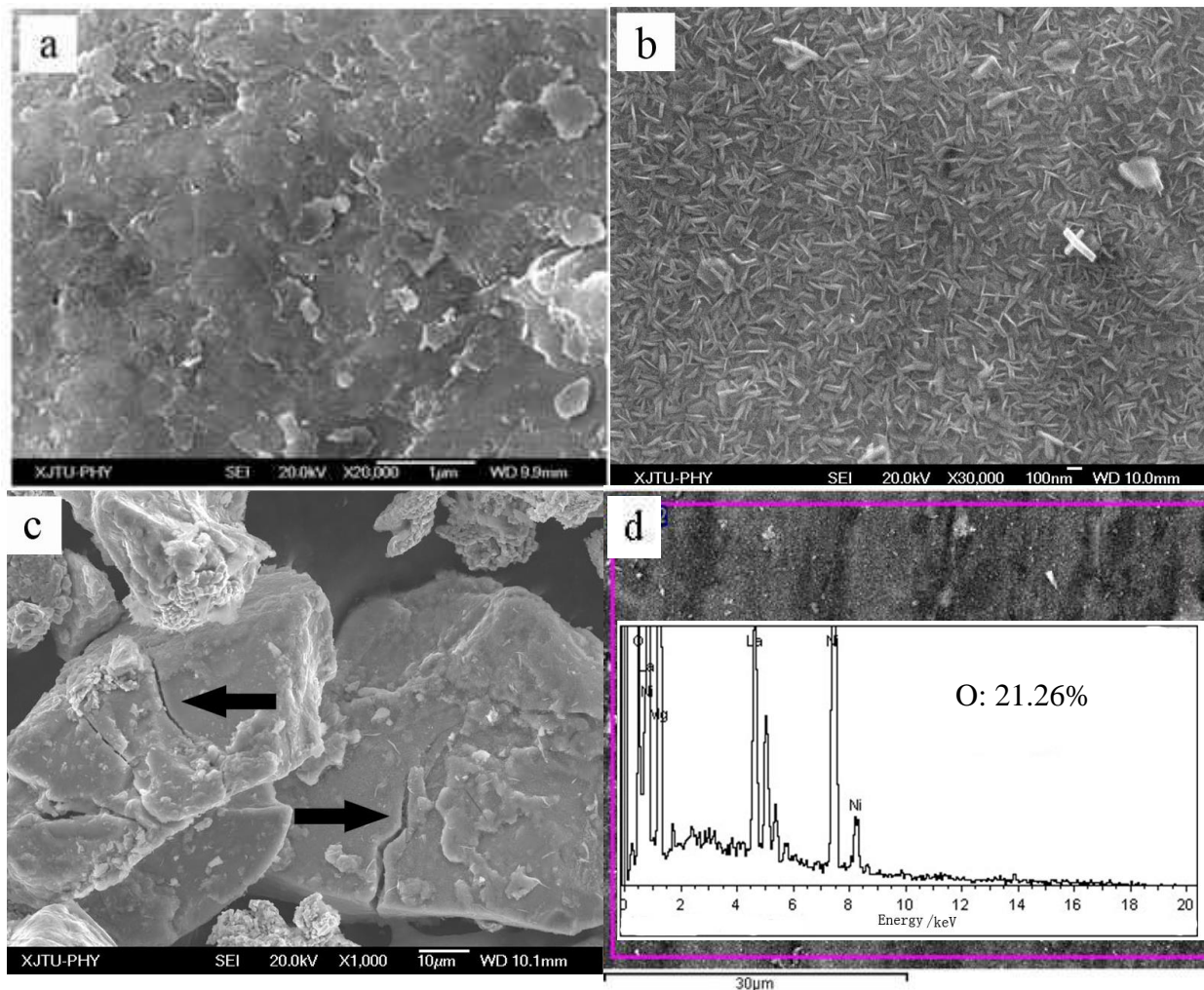


**Figure 3.** SEM image of  $(Mg_{65}Ni_{27}La_8)$  amorphous samples without G/A charged–discharged for: a: 0 cycle, b and c: 50 cycles, d: EDS patterns of  $(Mg_{65}Ni_{27}La_8)$  amorphous samples without G/A charged–discharged for 50 cycles.

SEM images of  $Mg_{65}Ni_{27}La_8$  amorphous samples with 0.2 mass fraction G/A after 0 (a), and 50 charge/discharge cycles (b and c), and EDS pattern of  $Mg_{65}Ni_{27}La_8$  amorphous samples with 0.2 mass fraction G/A after 50 charge/discharge cycles (d) are displayed in Fig. 4. The G/A composites cover the whole surface of the electrode, revealing good surface modification and uniform distribution. After 50 cycles, the G/A coating on the surface of the electrode remains, and the oxygen content is only 9.83%, suggesting that the G/A composite prevents the electrode from pulverizing and oxidizing.

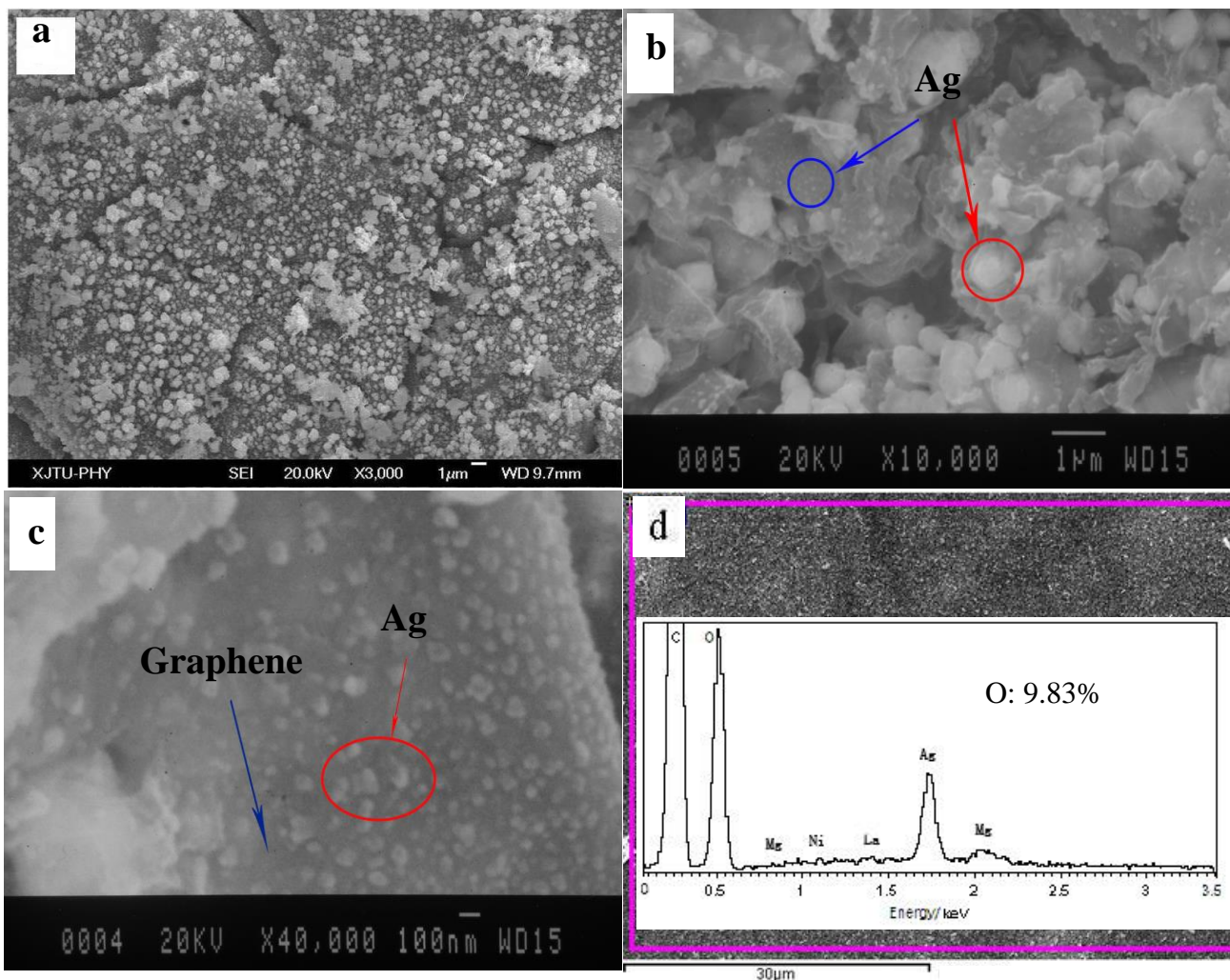


**Figure 4.** SEM image of  $(\text{Mg}_{65}\text{Ni}_{27}\text{La}_8)$  amorphous samples with 0.2 G/A charged–discharged for: a: 0 cycle, b and c: 50 cycles, d: EDS patterns of  $(\text{Mg}_{65}\text{Ni}_{27}\text{La}_8)$  amorphous samples with 0.2 G/A charged–discharged for 50 cycles.

Fig. 5 shows HRTEM images and electron diffraction patterns of amorphous  $\text{Mg}_{65}\text{Ni}_{27}\text{La}_8$  sample after 4 (a), 10 (b), 30 (c) and 50 charge/discharge cycles (d). The amorphous phase gradually crystallizes with additional cycling, corresponding to the capacity degradation of the electrode. A uniform amorphous structure remains after 4 charge/discharge cycles. (The micro-structure of short-range order is about 1-2 nm in Fig. 5 (a)). Ten charge/discharge cycles for the amorphous electrode samples results in formation of a nano-crystalline  $\text{MgH}_2$  phase with average grain size about 5–10 nm (Fig. 2 b and Fig. 5 b). After 30 charge/discharge cycles a coarser grained crystalline  $\text{Mg}_2\text{NiH}_4$  and  $\text{LaH}_2$  phase appears, with average grain size in the range of 20–30 nm (Fig. 2 c and Fig. 5 c). The amorphous electrodes are almost completely crystallized after 50 charge/discharge cycles, and the

stable  $\text{Mg}_2\text{NiH}_4$ ,  $\alpha\text{-Mg}$ ,  $\text{MgH}_2$ ,  $\text{Mg}_2\text{NiH}_{0.3}$  and  $\text{LaH}_2$  phases with the biggest grain size about 100-120 nm (Fig. 2 d and Fig.5 d) are present.

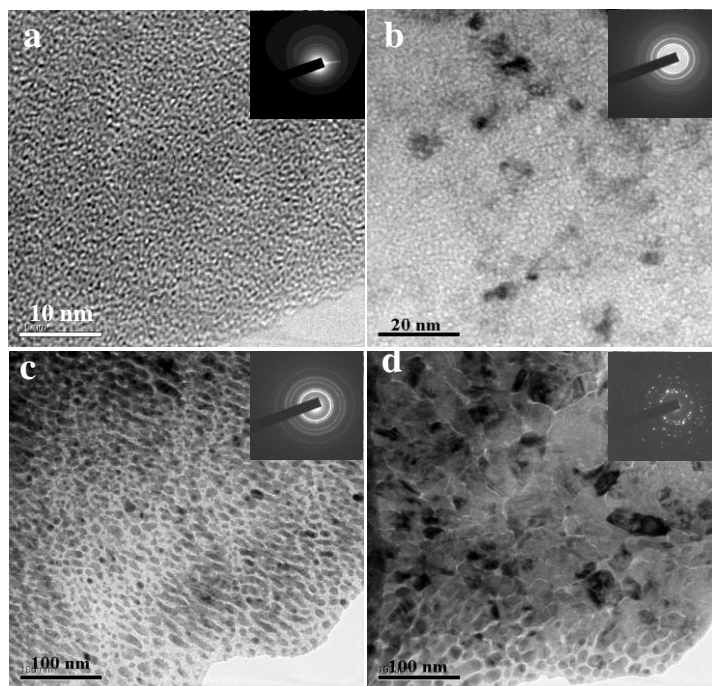


**Figure 5.** HRTEM image and electron diffraction pattern of amorphous ( $\text{Mg}_{65}\text{Ni}_{27}\text{La}_8$ ) sample charged/discharged for a: 4 cycles, b: 10 cycles, c: 30 cycles, d: 50 cycles.

HRTEM images and electron diffraction patterns of amorphous  $\text{Mg}_{65}\text{Ni}_{27}\text{La}_8$  with 0.2 mass fraction G/A sample after 10 (a), 30 (b) and 50 charge/discharge cycles (c) are shown in Fig. 6. The amorphous electrode alloys coated by G/A also gradually crystallize as cycling proceeds, but the crystallization process is reduced compared to the uncoated electrode. The amorphous electrode samples are almost completely crystallized and the stable  $\text{Mg}_2\text{NiH}_4$ ,  $\alpha\text{-Mg}$ ,  $\text{MgH}_2$  and  $\text{LaH}_2$  phases are present with the grain size about 40-60 nm (Figs. 6 c) after 50 charge/discharge cycles.

From the experimental results above, Fig. 7 A shows the schematic model of particle pulverization and surface oxidation/corrosion of Mg-based electrode alloys during hydrogenation/dehydrogenation cycling. The degradation process of the Mg-based alloy electrode with no G/A consists of three continuous stages: particle pulverization, Mg oxidation, and oxidation-passivation (Fig. 7 A) [26-28]. After the initial 6–12 cycles, the electrode particles are gradually pulverized to smaller particles, resulting in fresh surface areas exposed to the KOH/LiOH solution. At the same time, magnesium on the electrode surface is oxidized to  $\text{Mg}(\text{OH})_2$  leading to a decrease in the amount of active elemental Mg. Next, in the Mg oxidation step (subsequent 15–25 cycles), further

oxidation of the electrode alloy occurs, especially for the active elements such as Mg. In this stage, elemental Mg is continually oxidized to  $\text{Mg}(\text{OH})_2$ , which forms a permeable passive layer, because magnesium is the most active element in the alloy, and the  $\text{Mg}(\text{OH})_2$  film is too loose to prevent the electrode from further corrosion/oxidation. In the last oxidation-passivation stage (after 35 cycles), the corrosion/oxidation of elemental Mg continues with a substantial loss of discharge capacity, and the  $\text{Mg}(\text{OH})_2$  layer on the electrode surface gradually becomes thicker with continued cycling. The formation of  $\text{Mg}(\text{OH})_2$  film decreases the diffusivity of hydrogen and the surface reaction kinetics of the electrode alloys. The combined actions of these factors cause a fast discharge-capacity loss for Mg-based alloy electrodes.

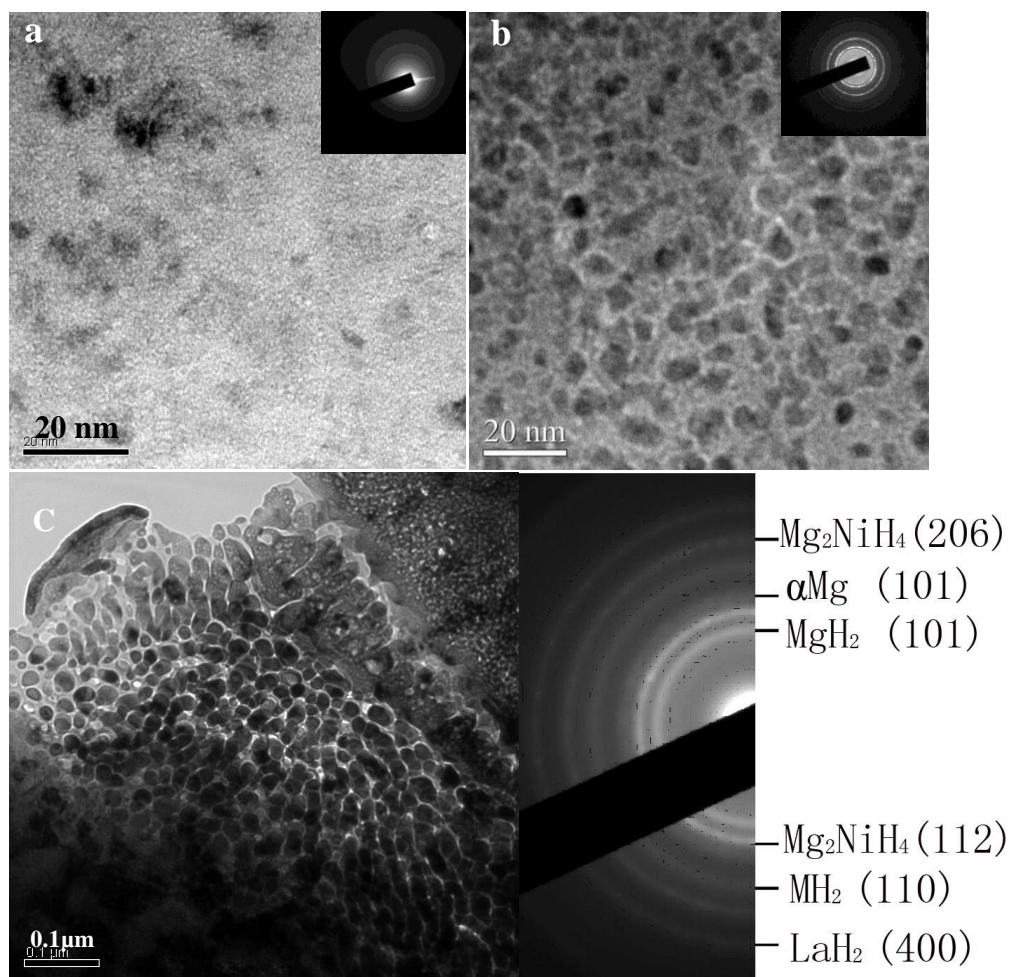


**Figure 6.** HRTEM image and electron diffraction pattern of amorphous ( $\text{Mg}_{65}\text{Ni}_{27}\text{La}_8$ ) with 0.2 G/A sample charged/discharged for a: 10 cycles, b: 30 cycles, c: 50 cycles.

Reducing oxidation and corrosion of the electrode alloys is essential to improve the electrochemical properties of Mg-based electrodes. Fig. 7 B shows our schematic diagram of the surface modification for Mg-based electrode alloy with G/A. We prepared Mg-Ni-La amorphous alloy by a melt-spin method, and deposited Ag nanoparticles onto graphene sheets to form a G/A surface coating. We then investigated Mg-Ni-La amorphous electrode alloys with different mass fractions of G/A nanocomposite. The surface modification using G/A reduces the contact resistance of the alloy, enhances the electrocatalytic activity of the electrode, and also improves the anti-corrosion and anti-oxidation properties of the electrodes.

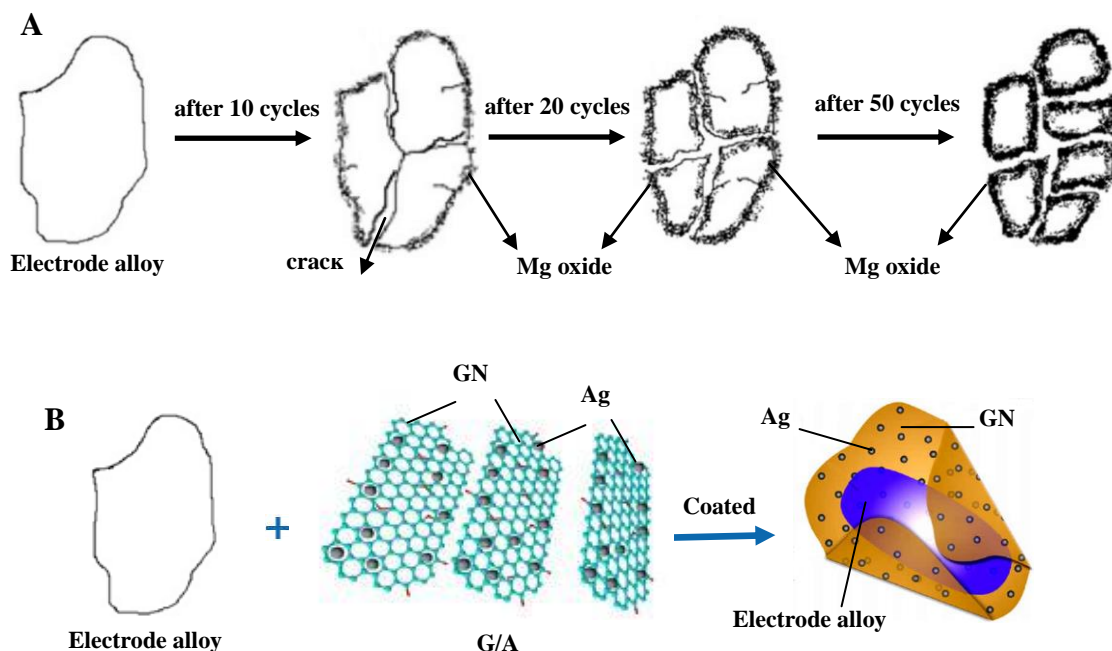


**Figure 7.** A: Schematic model of disintegration and surface oxidation for Mg-based electrode alloys during charge/discharge cycling and B: The schematic diagrams of Surface modification for Mg-based electrode alloy with G/A

Modification with the G/A nanocomposite improves electrochemical performance parameters of the electrode alloys, such as limiting current density, discharge capacity, discharge potential characteristics, and cycle stability [22]. We think that G/A nanocomposites react with Mg-Ni-La amorphous alloy particles and may donate electron density to the electrode surface during high-energy ball milling. The chemical states of elemental Mg and G/A–Mg interaction that form on the electrode surface are modified by the electrons trapped on the alloy surface. The surface modification thereby partially prevents the formation of  $\text{Mg}(\text{OH})_2$  on the electrode surface and increases the active sites for

hydrogen absorption/desorption. All of these factors increase the anti-corrosion and anti-oxidation properties of the electrode alloys and improve the discharge capacity and cycle stability of the electrodes.

Fig. 8 is attempted to give a further explanation of the charge/discharge process, which shows a schematic illustration of electrochemical hydrogen absorption/desorption. The surface oxide layer on the hydride particle is confirmed to prevent both the hydrogen reaction on the interface of electrolyte-electrode and hydrogen diffusion. Therefore, even after the alloy powders have been cracked because of the contraction and expansion of the particle during the charge-discharge process [29], the newly exposed surface exerts little effect on the electrode properties, as the fresh particle surface will be corroded very quickly. However, the G/A coating layer can provide both a pathway for hydrogen diffusion and active sites for the redox reaction of hydrogen [30], as shown in Fig. 8. All of these factors result in a substantial improvement of the discharge capacity by about  $250 \text{ mAhg}^{-1}$  in each cycle (after activation) for Mg-Ni-La electrode with 0.2 G/A (see Fig. 1 a and d).

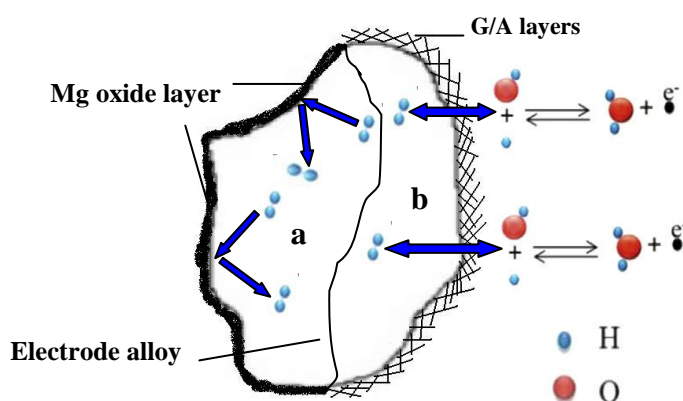


**Figure 8.** The charging/discharging diagram of  $(\text{Mg}_{65}\text{Ni}_{27}\text{La}_8)$  amorphous samples for a: without G/A and b: after coating with G/A

#### 4. CONCLUSIONS

G/A is used to modify the  $\text{Mg}_2\text{NiH}_4$  via mechanical milling, to improve the electrochemical properties of  $\text{Mg}_2\text{Ni}$ -based hydrides. The influence of G/A coating layer on the microstructural evolution and electrochemical properties of the Mg-Ni-La hydride is investigated in detail. SEM and EDS reveal that G/A composites significantly prevent the electrodes from pulverizing and oxidizing. The oxygen content is reduced from 21.26% to 9.83% after 50 cycles for Mg-Ni-La electrode coated with 0.2 mass fraction G/A. HRTEM shows that the amorphous samples are almost completely crystallized and stable  $\text{Mg}_2\text{NiH}_4$ ,  $\alpha\text{-Mg}$ ,  $\text{MgH}_2$  and  $\text{LaH}_2$  phases with the grain size about 40-60 nm are

present after 50 charge/discharge cycles, further confirming that the amorphous structure of electrodes coated by G/A also gradually crystallize as cycling proceeds. However, the crystallization process is much slower on the G/A-coated electrode than on the uncoated electrode. The surface modification enhances the electrocatalytic activity of the alloy and reduces oxidation and corrosion of the alloy. Furthermore, the G/A coating provides both active sites for the redox reaction of hydrogen, and a pathway for hydrogen diffusion. All of these factors result in a substantial improvement of the discharge capacity by about  $250 \text{ mAhg}^{-1}$  in each cycle (after activation) for Mg-Ni-La electrode with 0.2 weight fraction G/A.

#### ACKNOWLEDGEMENTS

This work was supported by the Natural Scientific Foundation of China (Grantno. 51503112, 51273096, 51373081), Natural Scientific Foundation of Shandong Province (Grantno.ZR2014EMM008, ZR2015EM008) and the Technology Development Projects of Qingdao city (Grantno.14-2-4-2-jch).

#### References

1. L. Schlapbach and A. Züttel, *Nature*, 414 (2001) 353.
2. H.D. Yoo, I. Shterenberg, Y. Gofer, G. Gershinsky, N. Pour and D. Aurbach, *Energy Environ. Sci.*, 6 (2013) 2265.
3. J. Muldoon, C.B. Bucur, A.G. Oliver, T. Sugimoto, M. Matsui, H.S. Kim, G.D. Allred, J. Zajicek and Y. Kotani, *Energy Environ. Sci.*, 5 (2012) 5941.
4. S. Rasul, S. Suzuki, S. Yamaguchi and M. Miyayama, *Electrochim. Acta*, 82 (2012) 243.
5. G. Gershinsky, H.D. Yoo, Y. Gofer and D. Aurbach, *Langmuir*, 29 (2013) 10964.
6. M. Bououdina, D. Grant and G.Walker, *Int. J. Hydrogen Energy*, 31 (2006) 177.
7. J.S. Xue, G.X. Li and Y.Q. Hu, *J. Alloys Compd.*, 307 (2000) 240.
8. L.J.Huang, G.Y. Liang, Z.B. Sun and D.C.Wu, *J. Power Sources*, 160 (2006) 684.
9. F.X. Wang, X.P. Gao and Z.W. Lu, *J. Alloys Compd.*, 370 (2004) 326.
10. M.Bououdina, D. Grant and G.Walker, *Int. J. Hydrogen Energy*, 31 (2006)177.
11. L.J. Huang, G.Y. Liang and Z.B. Sun, *J. Alloys Compd.*, 421 (2006) 279.
12. X.D. Wei, P. Zhang, H. Dong, Y.N. Liu, J.W. Zhu and G. Yu, *J. Alloys Compd.*, 458 (2008) 583.
13. C.Y. Wang, D.H. Bradhurst and S.X. Dou, *J. Alloys Compd.*, 285 (1999) 267.
14. W.Z. Shen, S.M. Han, Y. Li, J. Yang and K. Xiao, *Mater. Chem. Phys.*, 132 (2012) 852.
15. F. Feng and D.O. Northwood, *Int. J. Hydrogen Energy*, 29 (2004) 955.
16. Y.F. Liu, H.G. Pan, M.X. Gao and Q.D. Wang, *J. Mater. Chem.*, 21 (2011) 4743.
17. T. Abe, S. Inoue, D. Mu, Y. Hatano and K. Watanabe, *J. Alloys Compd.*, 349 (2003) 279.
18. Z.P. Guo, Z.G. Huang, K. Konstantinov, H.K. Liu and S.X. Dou, *Int. J. Hydrogen Energy*, 31 (2006) 2032.
19. D.C. Wu, L. Li, G.Y. Liang, Y.L. Guo and H.B. Wu, *J. Power Sources*, 189 (2009) 1251.
20. L.Z. Ouyang, Z.J. Cao, H. Wang, J.W. Liu, D.L. Sun, Q.A. Zhang and M. Zhu, *J. Alloys Compd.*, 586 (2014) 113.
21. W. Oelerich, T. Klassen and R. Bormann, *J. Alloys Compd.*, 315 (2001) 237.

22. L.J. Huang, Y.X. Wang, Z. Huang, J.G. Tang, Y. Wang, J.X. Liu, J.Q. Jiao, J.Q. Liu and A. L. Belfiore, *J. Power Sources*, 269 (2014) 716.
23. C. Iwakura, H. Inoue, S.G. Zhang and S. Nohara, *J. Alloys Compd.*, 293–295 (1999) 653.
24. L. Aymard, C. Lenain, L. Courvoisier, F. Salver-Disma and J.M. Tarascon, *J. Electrochem.Soc.*, 146 (1999) 2015.
25. B. Liao, Y.Q. Lei, L.X. Chen, G.L. Lu, H.G. Pan and Q.D. Wang, *J. Power Sources*, 129 (2004) 358.
26. Y.F. Liu, H.G. Pan, M.X. Gao, Y.Q. Lei and Q.D. Wang, *J. Electrochem. Soc.*, 152 (2005) A1089.
27. Y.F. Liu, H.G. Pan, M.X. Gao, Y.Q. Lei and Q.D. Wang, *J. Alloys Compd.*, 403 (2005) 296.
28. Y.F. Liu, H.G. Pan, M.X. Gao, H. Miao, Y.Q. Lei and Q.D. Wang, *Int. J. Hydrogen Energy*, 33 (2008) 124.
29. M.X. Gao, S.C. Zhang, H. Miao, Y.F. Liu and H.G. Pan, *J. Alloys Compd.*, 489 (2010) 552.
30. J.L. Luo and N. Cui, *J. Alloys Compd.*, 264 (1998) 299.

© 2016 The Authors. Published by ESG ([www.electrochemsci.org](http://www.electrochemsci.org)). This article is an open access article distributed under the terms and conditions of the Creative Commons Attribution license (<http://creativecommons.org/licenses/by/4.0/>).